Supplementary Information

High-speed 4D computed tomography for uncovering the dynamics of oil uptake in deep-fried food products

U. Verma[1], I. M. Riley[2], B. Lukić[4], L. Broche[4], P. Verboven[1*], J. A. Delcour[2], B. M. Nicolaï[1,3]

[1]Division BIOSYST-MeBios, KU Leuven, Willem de Croylaan 42, B-3001, Leuven, Belgium

[2]Laboratory of Food Chemistry and Biochemistry, KU Leuven, Kasteelpark Arenberg 20, B-3001 Leuven, Belgium.

[3]Flanders Centre of Postharvest Technology, Willem de Croylaan 42, B-3001 Leuven, Belgium

[4]European Synchrotron Radiation Facility, CS 40220, Grenoble F-38043, France

ujjwal.verma@kuleuven.be (U. Verma), isabellamaria.riley@kuleuven.be (I. M. Riley), bratislav.lukic@esrf.fr (B. Lukić), broche@esrf.fr (L. Broche), pieter.verboven@kuleuven.be (P. Verboven), jan.delcour@kuleuven.be (J.A. Delcour), bart.nicolai@kuleuven.be (B. Nicolai)

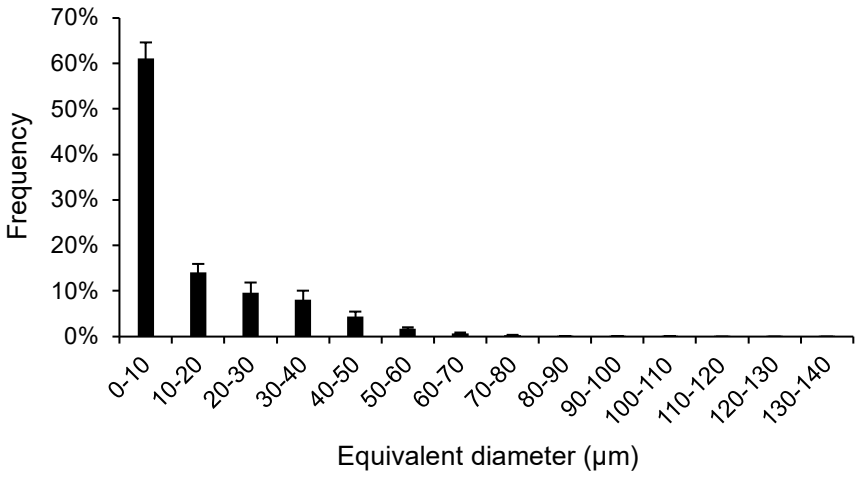

Figure S1. Pore size distribution of gas pores in WFD sample before deep-frying. Values averaged over 3 representative volumes (1.54 X 1.54 X 1.54 mm^3).

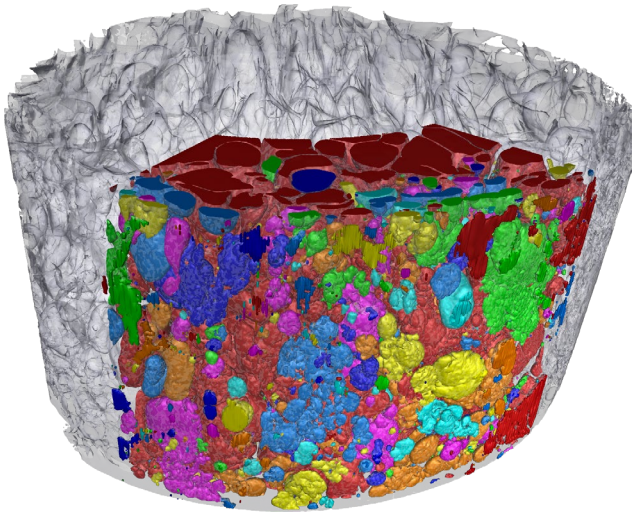

Figure S2. 3D volume render of labelled pore space inside WFD samples deep-fried at 180 °C after 56 s of frying. The same label colour of adjacent objects depicts a connected pore network. Pores present in the outer crust regions were distinctly disconnected to the core regions of the sample.

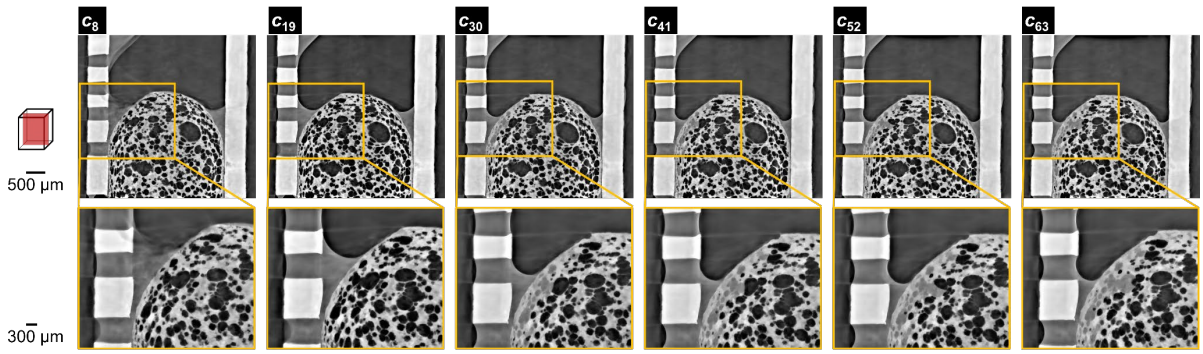

Figure S3. Vertical cross-sections of reconstructed images depicting oil uptake during cooling for WFD samples deep-fried at 180 °C, inset images highlight the surface oil being pulled into the structure. Rows correspond to the 10 s time intervals depicting progression in time. [Scale bar indicated in µm; time labels c_i denote observations during frying period; subscripts denote the time in s].

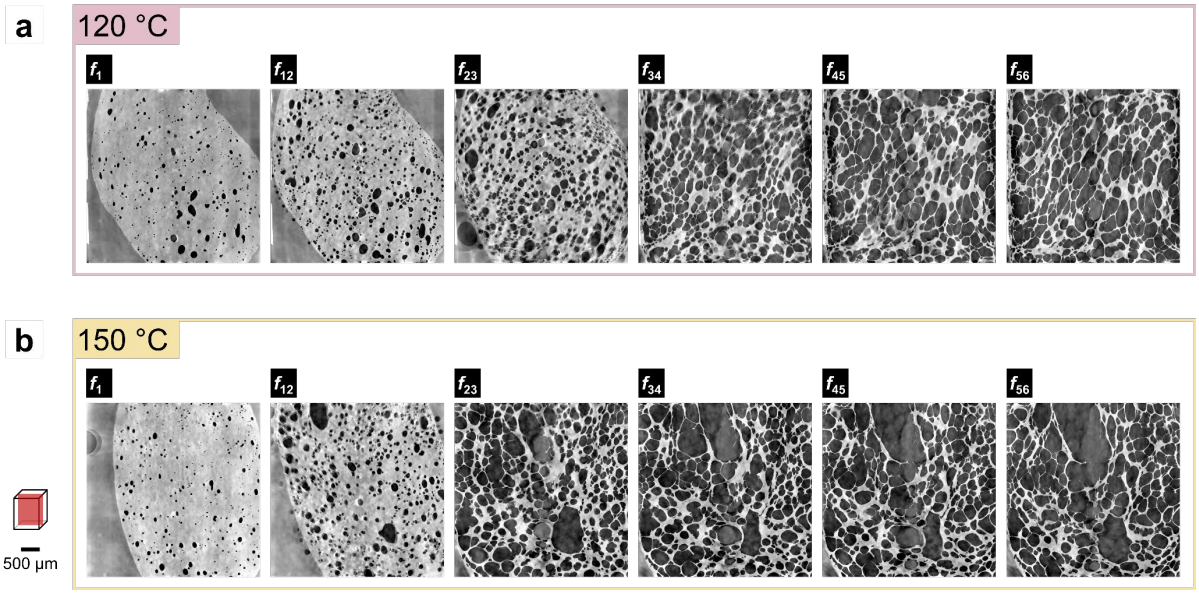

Figure S4. Vertical cross-sections of reconstructed images highlighting structural deformation for WFD samples during in-situ deep-frying at lower oil temperatures. a – 120 °C and **b** – 150 °C; Rows correspond to the 10 s time intervals depicting progression in time. [Scale bar indicated in µm; time labels f_i denote observations during frying period; subscripts denote the time in s].

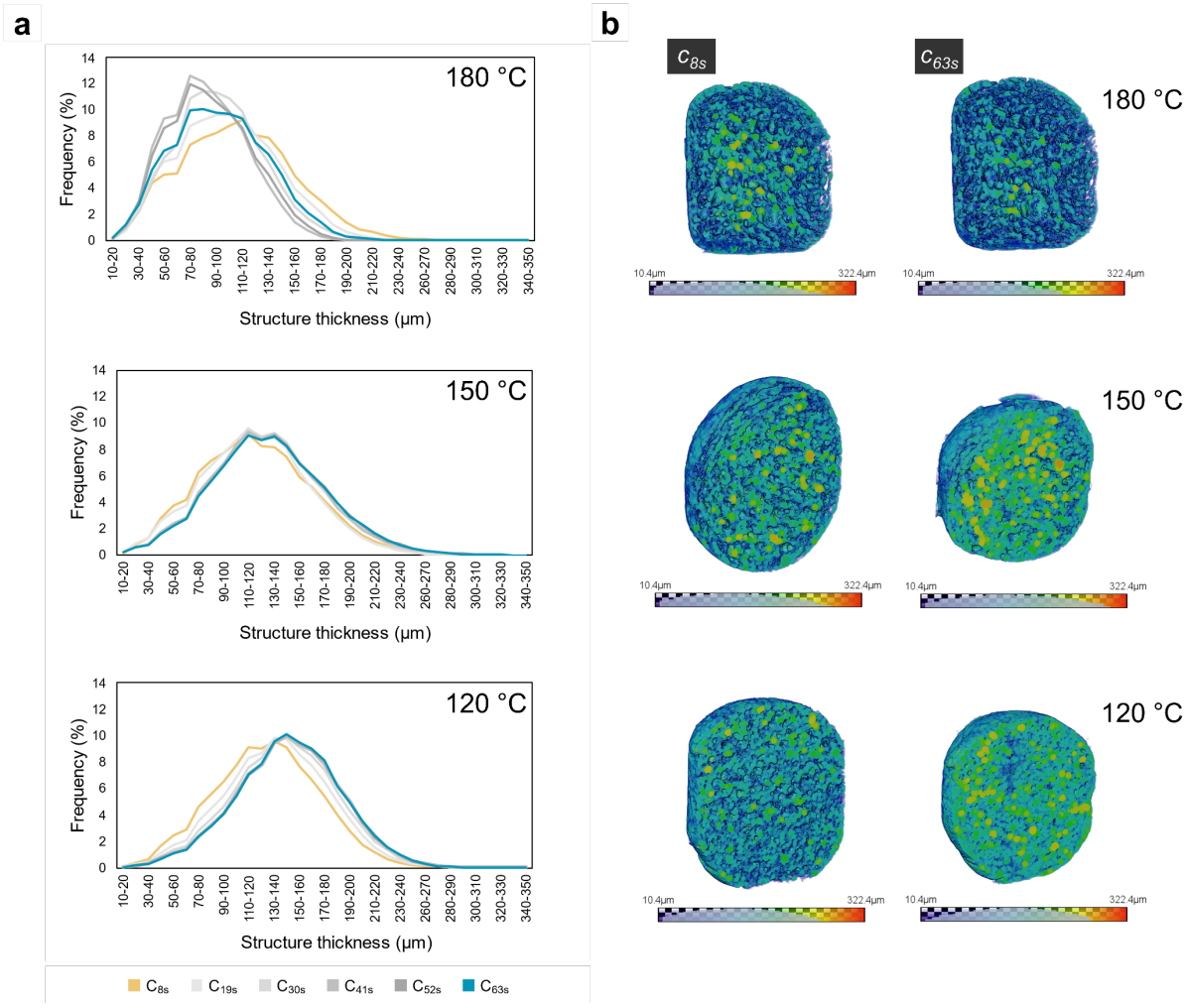

Figure S5. Evolution of structure thickness of the solid matrix for WFD samples deep-fried at 180, 150 and 120 °C during post-frying cooling. a Structure thickness distribution; **b** 3D volume renders of the starch-gluten matrix with an applied colour map correlated with local thickness, thin regions are at the lower (indigo-colour) end of the spectrum and thicker regions at the higher (red-colour) end. [Time labels c_j denote observations during cooling after retraction from oil; subscripts denote the time in s]

Table S1. Average structure thickness of the solid matrix for WFD samples deep-fried at 180, 150 and 120 °C during post-frying cooling.

Oil temperature	Time (s)	Structure thickness (μm)
180 °C	8	110.20(4.52)
	19	102.16(3.95)
	30	95.83(3.85)
	41	86.21(3.52)
	52	88.72(3.66)
	63	96.50(5.00)
150 °C	8	119.66(6.00)†
	19	122.55(6.65)†
	30	127.96(6.16)
	41	128.69(10.03)
	52	131.07(10.29)
	63	131.15(10.06)
120 °C	8	129.20(1.97)
	19	136.99(1.90)
	30	142.91(3.67)
	41	146.77(3.93)
	52	146.87(3.69)
	63	147.38(5.50)

Values represent the mean (n = 3, †n = 2) with standard deviation presented in brackets.

Table S2. Ilastik out-of-bag error.

	C_{8s}	C_{19s}	C_{30s}	C_{41s}	C_{52s}	C_{63s}
180 °C	0.003838	0.002678	0.003972	0.005873	0.005334	0.008872

Conventional intensity-based thresholding methods for image segmentation failed to generate acceptable results. To overcome this, machine learning based pixel classification was performed using Ilastik (see Methods). Given the variability of structures in the dataset across all trained models, the quality of prediction was visually inspected in combination with the out-of-bag (OOB) error (which provided a performance indication of the trained model) to determine when the model was acceptably trained. OOB error represents a metric for the prediction error by which a pixel can be incorrectly characterized into one of the four classes. These values were interpreted with caution as the OOB error is susceptible to variation across different trained models due to its dependence on annotated pixels. Though particular care was taken during manual annotation (regarded as training data) of pixels for the different classes in each trained model, it was not possible to standardize the number of pixels annotated across models due to the changing structure morphology between repetitions.